VACUUM BOUNCING DYNAMICS DOMINATED BY VAN DER WAALS FORCES IN MEMS RELAYS

B. Ma[1], Z. You[1], and Y. Ruan[1]
[1]Department of Precision Instrument, Tsinghua University, Beijing, CHINA

ABSTRACT

This paper reports a MEMS relay with high reliability, in which van der Waals forces will be used, for the first time, to significantly suppress the vacuum contact bouncing. The dynamic analysis has been carried out by modeling the microcantilever as a multi-segment beam. In the model, van der Waals forces as an adhesive force replace air damping to represent the suppression term. In combination with a dual-pulse actuation waveform implemented by simple logic circuits, the contact bounces were eventually eliminated by making a soft landing.

INTRODUCTION

The dynamic behaviors of MEMS relays are known to suffer from discrete contact bounces during their closing, which will lead to extended switching time, contact wear, and contact welding [1,2]. A lot of work has been done to understand the nature of contact bouncing. McCarthy et al. developed a time-transient finite difference model based on Euler-Bernoulli beam theory, which included squeeze-film damping and a linear contact spring to analysis the dynamic behavior of a contact RF-MEMS switch [3]. Decuzzi et al. adopted a similar approach, but included van der Waals force to represent the attractive force [4]. Tung et al. proposed a multiple eigenmode model and used laser Doppler vibrometer to analyze a cantilever switch response [5]. 2D and 3D nonlinear dynamic models have also been developed to describe the transient bouncing dynamics of the contact-type MEMS devices [6,7]. However, the dynamic bouncing will be greatly exacerbated in vacuum without air damping. In the nanometer distances, van der Waals forces, which tend to be preventive as an adhesion factor, become comparable with the driving force and may therefore significantly influence the dynamics of MEMS relays. This paper provides a detailed analysis of the vacuum bouncing dynamics dominated by van der Waals forces, and eventually eliminates contact bounces by driving with a dual-pulse actuation waveform.

MODELING AND SIMULATION

Multi-segment cantilever

The proposed MEMS relay is fabricated through a bulk-silicon process based on silicon-on-insulator (SOI) anodic bonding technology, which significantly improves the device reliability and consistency [8]. As shown in Fig. 1(a), the relay structure is a novel cantilever beam with hollow suspended spring, which is used to limit spring stiffness and enhance relay stabilization. The electrostatic parallel-plate actuator switches the relay on and off. And the contact levers are connected between the driving plate and the contact bar. Gold is chosen as the contact material because of its minimal contact resistance. Table 1 presents the specific geometric parameters of the proposed MEMS relay and the equivalent multi-segment cantilever.

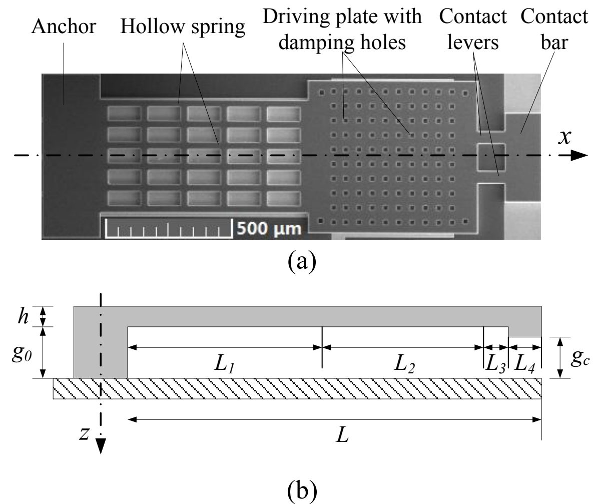

(b)

Figure 1: Schematic of the cantilever MEMS relay. (a) SEM image. (b) The equivalent multi-segment cantilever.

Table 1. Geometric parameters of the proposed MEMS relay and the equivalent multi-segment cantilever.

Parameters	Value
Structure thickness (h)	24 μm
Air gap height (g_0)	3 μm
Contact gap height (g_c)	2.4 μm
Driving plate ($L_2 \times W_2$)	640 μm × 580 μm
Hollow spring ($L_1 \times W_h$)	630 μm × 370 μm (coupled with six 20 μm wide microbeams)
Contact levers ($L_3 \times W_c$)	100 μm × 50 μm
Contact bar ($L_4 \times W_4$)	140 μm × 340 μm
First segment width (W_1)	132 μm
Second segment width (W_2)	580 μm
Third segment width (W_3)	100 μm
Fourth segment width (W_4)	340 μm

The MEMS relay is a very non-uniform cantilever beam, which cannot be modeled by the conventional lumped parameter. However, due to its symmetry, the MEMS relay can be modeled as a virtual line beam on its axis with different stiffness along the length direction, as shown in Fig. 1(b). According to the Euler-Bernoulli beam theory, the cantilever beam can be divided into four solid segments with different width that is equal to the sum of the physical width, and this has been confirmed and corrected by a 3D solid mechanics model. Hence, the presented 1D multi-segment cantilever beam can be used to model the non-uniform MEMS relay and give some details along the width direction. The four segments are denoted by L_1, L_2, L_3 and L_4, which represent the lengths of the hollow spring, driving plate, contact levers and contact bar. Correspondingly, the width of the cantilever beam $W(x)$ can be expressed as:

$$W(x)=\begin{cases} W_1, & x\in[0,L_1] \\ W_2, & x\in[L_1,L_1+L_2] \\ W_3, & x\in[L_1+L_2,L-L_4] \\ W_4, & x\in[L-L_4,L] \end{cases}. \quad (1)$$

Governing equation

The classical Euler-Bernoulli theory can be employed for modeling. In vacuum, the air damping effects can be ignored; hence, the microbeam equation of motion can be expressed as follows:

$$\rho A_0\frac{\partial^2 z}{\partial t^2}+EI\frac{\partial^4 z}{\partial^4 x}=F_e+F_a-F_c. \quad (2)$$

Where ρA_0 is the mass per unit length, EI is the flexural rigidity. F_e is the electrostatic force, F_a is the adhesion force caused by van der Waals forces, and F_c is the contact force. The dynamic response of the system is derived by solving the above equation for $z(x,t)$ with the initial and boundary conditions described below:

$$z(0,t)=0,\quad \frac{\partial z}{\partial x}(0,t)=0. \quad (3)$$

The electrostatic force F_e is generally introduced by the parallel-plate electrostatic actuator, corrected by the first-order fringing field effect.

$$F_e=\frac{\varepsilon_0 W_2 V_e^2}{2(g_0-z)^2}(1+0.65\frac{g_0-z}{W_2}),\quad x\in[L_1,L_1+L_2] \quad (4)$$

Where ε_0 is the permittivity of vacuum; g_0 is the initial gap height; and V_e is the driving voltage. The electrostatic load is applied only on the segment labeled L_2.

The contact substrate can be modeled as an elastic foundation. When the contact bar comes into contact with the substrate, the deformation of the foundation springs produces the contact force that can be approximated by a linear spring model.

$$F_c=k_c(z-g_c)\cdot H(z-g_c),\quad x\in[L-L_4,L] \quad (5)$$

Here, the Heaviside function $H(z-g_c)$ ensures the contact force applied only at those locations where $z\geq g_c$. The contact spring constant k_c take an empirical value, which ensures that the substrate deformation is small.

Van der Waals forces

Van der Waals forces become significant in nanometer distances, and pose a fundamental limit to the adhesion between micromachined surfaces. The normal van der Waals force is generated by the temporary dipole moment produced by the instantaneous positions of electrons in a molecule. The temporary dipole polarizes the electron distribution of a nearby molecule, and creates attractive dispersion energy proportional to $1/r^6$, where r is the distance between the molecules. The normal van der Waals force mainly governs at separations less than 10nm. For larger separations greater than 50nm, the Casimir force or retarded van der Waals force plays a major role, and the interaction energy between molecules becomes proportional to $1/r^7$. A gradual transition from normal to retarded van der Waals forces occurs between theses separations. Gold surface roughness is typically 2-5nm, which corresponds to the surface separation of 10-30nm. Therefore, the adhesion of gold surfaces is due to forces in the transition region between non-contacting areas.

The van der Waals forces between two smooth parallel surfaces can be expressed as:

$$F_a=\frac{AW_4 g_f}{6\pi(g_c-z)^3},\quad x\in[L-L_4,L]. \quad (6)$$

The Hamaker constant $A=4\times10^{-19}J$, and g_f is a function based on separation distance that describes the transition from normal to retarded van der Waals forces [10].

$$g_f=\Bigg[1-2\frac{g_c-z}{c}+6\frac{(g_c-z)^2}{c^2}+12\frac{(g_c-z)^3}{c^3} -12\frac{(g_c-z)^3}{c^4}(g_c-z+c)\ln\left(1+\frac{c}{g_c-z}\right)\Bigg] \quad (7)$$

Where $c=3.1\lambda/2\pi$, the coefficient 3.1 is to make the correction function match the Casimir and Polder function. λ denotes the characteristic wavelength of interaction, often assumed to be about 100 nm.

Introducing the following dimensionless parameters:

$$\hat{x}=\frac{x}{L},\quad \hat{z}=\frac{z}{g_0},\quad \hat{t}=\frac{t}{T},\quad T=\sqrt{12\rho L^4/Eh^2},\quad \beta=\frac{g_c}{g_0}$$
$$\alpha_1=\frac{6\varepsilon_0 L^4}{Eh^3 g_0^3},\quad \alpha_2=\frac{2AL^4}{\pi Eh^3 g_0^4},\quad \hat{k}_c=\frac{12L^4 k_c}{Eh^3}. \quad (8)$$

Where h represents the beam thick; $I=W(x)h^3/12$ is the second moments; T is the time scale constant. Then, the dimensionless equation of motion is

$$\frac{\partial^2 z}{\partial t^2}+\frac{\partial^4 z}{\partial^4 x}=\alpha_1\frac{W_2}{W(x)}\frac{V_e^2}{(1-z)^2}(1+0.65\frac{1-z}{W_2/g_0}) +\alpha_2\frac{W_4}{W(x)}\frac{g_f}{(\beta-z)^3}-\frac{k_c}{W(x)}(z-\beta)H(z-\beta) \quad (9)$$

RESULTS AND DISCUSSION

Finite element simulation

Modeling and solution is implemented by COMSOL Multiphysics. In order to confirm the validity of the 1D multi-segment model, we compared the simulated dynamic pull-in voltage with the static result obtained by a 3D model. The dynamic pull-in voltage of 17.2V is about 10% lower than the static value, which is in good agreement with the results of the reference [11]. Figure 2 shows the dynamic response of the multi-segment cantilever, in which the pull-in time is approximately 49.3μs when the applying voltage is 1.2 times the pull-in voltage.

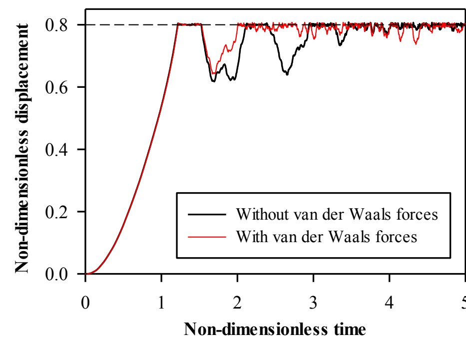

Figure 2: Simulated contact bouncing dynamics of the MEMS relay driving by 1.2 times the pull-in voltage.

Experimental results

The output voltage bounces were obtained by an oscilloscope. The relay was placed in parallel with a 1k resistor and a 2V voltage source, and then in series with a 1k resistor to limit the maximum load current of 2mA. The driving voltage was set to be 1.2 times the pull-in voltage. The measurements were carried out in a vacuum chamber, which ensures vacuum degree can reach less than 10^{-4}Torr. The output voltages curves are shown in Fig. 3. When the contact electrodes are solid, the number of the contact bounces is 6 times, less than the 9 times of the grid contacts. Thus, the output voltage bounces significantly suppressed by the increase of contact area. At the same time, the contact bounces greatly prolong the switching-on time and strongly deteriorate the reliability of relay closing.

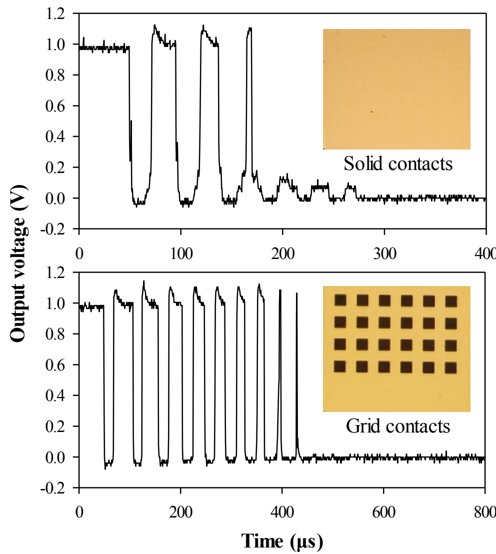

Figure 3: Vacuum output voltage bounces of solid and grid contacts driving by 1.2 times the pull-in voltage.

The transient contact behavior was measured by a Laser Doppler Vibrometer (LDV). In the experiments, laser spot was projected on the center of the contact bar, and then measured the displacement of this point. The transient displacement curves were obtained by an oscilloscope when MEMS relays were actuated by the driving voltage. Figure 4 shows the displacement bounces driving by 1.2 times the pull-in voltage. When the contact electrodes are solid, the number of the contact bounces is about 8 times, less than the 11 times of the grid contacts. The number of displacement bounces is two times more than the voltage bounces; this is because the displacement bounces are too small to change the output voltage.

The vacuum contact bouncing is mainly dominated by van der Waals forces. Van der Waals forces are proportional to the contact area and govern at separations of 10nm to 50nm. With the effective contact area increasing, the contact bounces are strongly suppressed. When the contacts are solid, which also means a larger contact area than the grid contacts, the magnitude and the number of the contact bounces are both significantly reduced. The switching-on time measured from the displacement curves is approximately 52μs, which is in good agreement with the simulated value of 49.3μs. However, due to the complexity of influence factors, the actual dynamic response is difficult to exactly match with the simulation results.

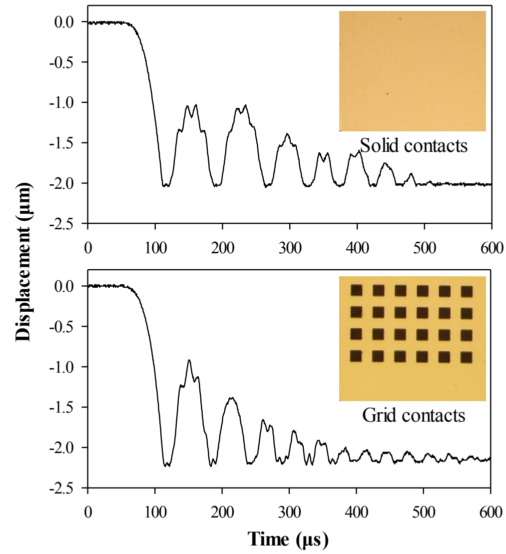

Figure 4: Vacuum displacement bounces of solid and grid contacts driving by 1.2 times the pull-in voltage.

We also measured the vacuum contact bouncing variations with the driving voltage. As shown in Fig.5, the contact bounces are significantly reduced with the increase of actuation voltage. However, when the driving voltage exceeds its limitation, the contacts will not be able to make contact effectively. Therefore, the contact bounces cannot be eliminated by simply increasing the driving voltage.

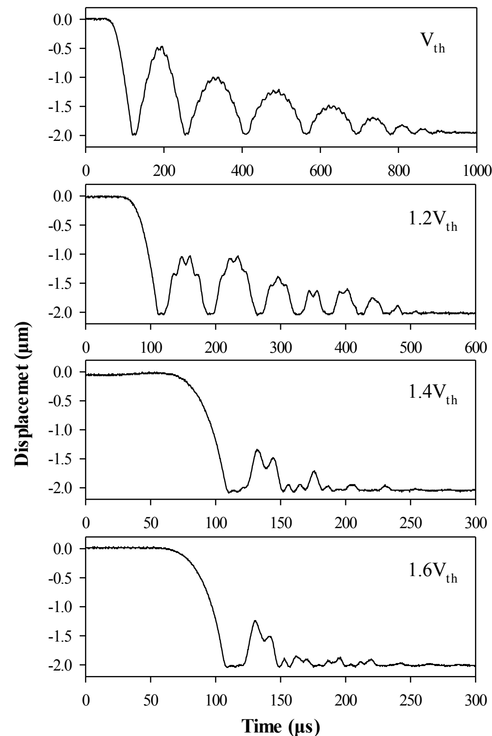

Figure 5: Vacuum contact bouncing variations with the driving voltage.

Soft-landing waveform

In this paper, we have implemented a dual-pulse actuation waveform to drive the cantilever beam for eliminating the vacuum contact bounces [12]. As shown in Fig. 6, the waveform consists of an actuation voltage pulse, a coast time, and a hold voltage, which can be easily generated by simple logic circuits. The actuation pulse has short duration and imparts kinetic energy necessary to close the MEMS relay. After the actuation voltage is turned off for a coast time, the restoring force slows the relay to near-zero velocity as it approaches the closed position. The hold voltage is then applied to hold the relay closed. The actuation voltage and the hold voltage have the same amplitude to simplify the dual-pulse waveform. The vacuum contact bounces have been eliminated by this dual-pulse actuation waveform and the switching-on time has also been shortened a lot.

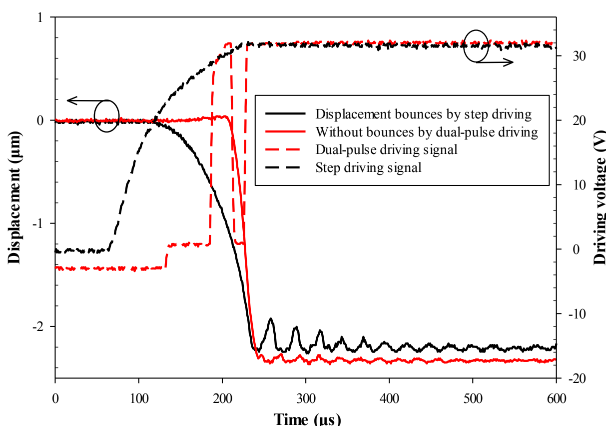

Figure 6: The step and dual-pulse actuation waveforms and the corresponding vacuum displacement curves.

CONCLUSION

The dynamic response of an electrostatically actuated MEMS relay has been analyzed by modeling the microcantilever as a multi-segment beam. This equivalent model focuses on the effects of electrostatic force and adhesion force caused by van der Waals forces. The model is well confirmed by the experimental results. In the nanometer scale, van der Waals forces pose a fundamental limit to the adhesion between micromachined surfaces. However, contact bouncing has become one of the most important failure mechanisms of MEMS relay in vacuum. This limitation can be used to replace air damping and suppress the vacuum contact bouncing to enhance the reliability of the MEMS relay. In combination with a dual-pulse actuation waveform implemented by simple logic circuits, the contact bounces were eventually eliminated by making a soft landing. In the future work, we would seek to find a balance between the suppression of adhesion and contact bounces to significantly improve the reliability of MEMS devices.

ACKNOWLEDGEMENTS

This work was supported by the State Key Laboratory of Precision Measurement Technology and Instruments (CHINA).

REFERENCES

[1] G. Subhash, A. D. Corwin, M. P. de Boer, "Evolution of Wear Characteristics and Frictional Behavior in MEMS Devices", *Tribol. Lett.*, vol. 41, pp. 177-189, 2011.

[2] C. M. Doelling, T. K. Vanderlick, J. Song, D. Srolovitz, "Nanospot Welding and Contact Evolution during Cycling of a Model Microswitch", *J. Appl. Phys.*, vol. 101, pp. 124303, 2007.

[3] B. McCarthy, G. G. Adams, N. E. McGruer, D. Potter, "A Dynamic Model, Including Contact Bounce, of an Electrostatically Actuated Microswitch, *J. Microelectromech. Syst.*, vol. 11, pp. 276-283, 2002.

[4] P. Decuzzi, G. P. Demelio, G. Pascazio, V. Zaza, "Bouncing Dynamics of Resistive Microswitches with an Adhesive Tip", *J. Appl. Phys.*, vol. 100, pp. 024313, 2006.

[5] R. C. Tung, A. Fruehling, D. Peroullis, A. Raman, "Multiple Timescales and Modeling of Dynamic Bounce Phenomena in RF MEMS Switches", *J. Microelectromech. Syst.*, vol. 23, pp. 137-146, 2014.

[6] V. Ostasevicius, R. Gaidys, R. Dauksevicius, "Numerical Analysis of Dynamic Effects of a Nonlinear Vibro-Impact Process for Enhancing the Reliability of Contact-Type MEMS Devices", *Sensors 2009*, vol. 9, pp. 10201-10216, 2009.

[7] Z.J. Guo, N. E. McGruer, G. G. Adams, "Modeling, Simulation and Measurement of the Dynamic Performance of an Ohmic Contact, Electrostatically Actuated RF MEMS Switch", *J. Micromech. Microeng.*, vol. 17, pp. 1899-1090, 2007.

[8] B. Ma, Z. You, Y. Ruan, S. K. Chang, G. F. Zhang "High-Power MEMS Relay Array with Improved Reliability and Consistency", *IEEE 18th Int. Conf. on TRANSDUCERS*, Alaska, June 21-25, 2015, pp. 2156-2159.

[9] F. W. Delrio, M. P. de Boer, J. A. Knapp, E. D. Reedy Jr, P. J. Clews, M. L. Dunn, "The Role of van der Waals Forces in Adhesion of Micromachined Surfaces", *Nat. Mater.*, vol. 4, pp. 629-634, 2005.

[10] A. Anandarajah, J. Chen, "Single Correction Function for Computing Retarded van der Waals Attraction", *J. Colloid Interface Sci.*, vol. 176, pp. 293-300, 1995.

[11] D. Elata, H. Bamberger, "On the Dynamic Pull-in of Electrostatic Actuators with Multiple Degrees of Freedom and Multiple Voltage Sources", *J. Microelectromech. Syst.*, vol. 15, pp. 131-140, 2006.

[12] H. Sumali, J. E. Massad, D. A. Czaplewski, C. W. Dyck, "Waveform Design for Pulse-and-Hold Electrostatic Actuation in MEMS", *Sensors Actuators A: Phys.*, vol. 134, pp. 213-220, 2007.

CONTACT

*Y. Ruan, tel: +86-10-6277-6000;
ruanyong@mail.tsinghua.edu.cn